Research paper

# Thermal decomposition of ammonium perchlorate and ammonium nitrate doped with nanometer $SO_4^{2-}/Fe_2O_3$ solid strong acid as catalyst



Xiaolan Song*†, Yi Wang**, Dan Song***, Chongwei An*, and Jingyu Wang*

*School of Chemical Engineering and Environment, North University of China, Taiyuan 030051, CHINA
Phone : +8615034015691
†Corresponding author : songxiaolan00@126.com

**School of Materials Science and Engineering, North University of China, Taiyuan 030051, CHINA

***China Ordnance Institute of Science and Technology, Beijing 100089, CHINA

Received : December 18, 2015 Accepted : February 9, 2016

## Abstract

Amorphous $Fe_2O_3$ nanoparticles were prepared by precipitation method. These nanoparticles were dipped in dilute sulfuric acid and then were calcined at different temperature. After that, the $SO_4^{2-}/Fe_2O_3$ solid strong acids with particle size of 30-40 nm were fabricated. Thermal analyses were recruited to probe the catalysis of nanometer $Fe_2O_3$ and nanometer $SO_4^{2-}/Fe_2O_3$ on decomposition of ammonium perchlorate (AP) and ammonium nitrate (AN). The results indicated that in case of AP, the peak temperature decreased by 35.1°C and 98.7°C in use of $Fe_2O_3$ and $SO_4^{2-}/Fe_2O_3$ as catalysts respectively. In the case of AN, the peak temperature lowered by 2.2°C and 18.0°C in use of $Fe_2O_3$ and $SO_4^{2-}/Fe_2O_3$ as catalysts respectively. DSC-IR analysis were performed to investigate decomposition products of [AP+3%$SO_4^{2-}/Fe_2O_3$] and [AN+3%$SO_4^{2-}/Fe_2O_3$]. The results demonstrated that [AP+3%$SO_4^{2-}/Fe_2O_3$] decomposed to $NO_2$, NOCl, $N_2O$, $HClO_4$, NO, HCl, and $H_2O$. For [AN+3%$SO_4^{2-}/Fe_2O_3$], the decomposition products were massive $N_2O$ and few $H_2O$. Note that there was no $NH_3$ presented in products, which meant that the decomposition reaction proceeded very completely. According to the detected products, the possible decomposition mechanism of AP and AN were derived. Meanwhile, the catalysis mechanisms of $SO_4^{2-}/Fe_2O_3$ were discussed in detail.

***Keywords*** : nanoparticles, solid strong acid, oxidizer, thermal decomposition, mechanism

## 1. Introduction

Ammonium perchlorate (AP) is the most common oxidizer used in composite solid propellants. It possesses of traits such as high oxygen balance, high energy, and excellent ignition and combustion properties. Due to the superior comprehensive performance, it is very difficult to replace AP by another oxidizer. Despite these advantages, there are still two problems in use. One is the hygroscopicity ; another is the much high decomposition temperature (>400°C). For hygroscopicity, it is not so serious that to block its application. However, too high decomposition temperature would deteriorate its reactions in condense and gas phase, i.e. pure AP consumes too many heats for sustaining its thermal decomposition. Therefore, adding some solid catalysts to decrease decomposition temperature of AP became a hot research topic since 2003[1)-5)]. In particular, nanometer catalysts exhibited higher catalysis than the micron catalysts[6)-10)]. For example, the AP/Al/hydroxyl terminated polybutadiene (HTPB) propellant was used in the first stage booster for launch of space shuttle, in which a great deal of $Fe_2O_3$ severed as combustion catalyst. Of course, there were many biting criticisms successively came from environmental experts because the combustion of those propellants discharged tons of HCl that caused serious air pollution. Different from AP based propellants, the propellants using ammonium nitrate (AN) as oxidizer are of the advantages such as non-toxic discharge, low

signature, and low sensitivities etc. HCl and oxychloride are not contained in combustion products of AN based propellants. Moreover, sensitivity of AN is much lower than that of AP. For example, pure AN can not be ignited by flame or heating even if the pressure accesses to 100 MPa. Its impact, friction, and shock sensitivities are closed to zero. Meanwhile, it explosion heat accesses 2640 J $g^{-1}$ and detonation velocity reaches 5270 m $s^{-1}$ ($\rho$ = 1.32 g $cm^{-3}$). For AP, its explosion heat is 1112.9 J $g^{-1}$ and its detonation velocity is only 3800 m $s^{-1}$. Thus, AN is a typical insensitive energetic material. Despite the super insensitivity, now it is very early to say we can use AN to replace AP. In practice, AN had not been applied as main oxidizer in the propellants of certain type of missile (or rocket, or booster), and it were just slightly used in some formulation of gas generation agents[11),12)]. What does results in this? Three inherent defects account for the uselessness of AN[13)]. Firstly, AN presents much more hygroscopicity than AP; secondly, phase transformation will occur at low temperature (30-80°C); the third, i.e. the most fatal factor, the ignition and combustion performance of AN based propellants are very poor. They burned so slowly that their combustion could not provide with sufficient thrust to boost the missile to fly at high speed. Therefore, the investigation about AN based propellants were in silence for many years.

At present, development of Insensitive Ammunition was becoming the "protagonist" in fields of military science and technology. Therefore, the studies about how to improve the performance of AN based propellants proliferated over the past five years. Especially, for better performance on the aspect of decomposition and combustion of AN, many studies were performed but the results were not satisfactory. In studies about AP, the researchers found that a good catalyst could always decrease the decomposition temperature by more than 100°C. However, this kind of results could not present in the studies about AN. If a catalyst could lower the decomposition temperature of AN by more than 10°C, we think it exhibited a good catalysis ability. For example, Naya investigated the catalysis of $MnO_2$ on thermal decomposition of AN[14)]. He found that the catalyst did not work at higher heating rate (20 °C $min^{-1}$); as the heating rate was lowered to 2 °C $min^{-1}$, its catalysis action was perceived, i.e. the DSC peak temperature of AN doped 4% $MnO_2$ decreased by 16°C comparing with that of pure AN; nevertheless, the propellant added $MnO_2$ as catalyst could not be ignited at low pressure (≤ 1 MPa). In the study of Popok, he used nano Al and $\gamma$-$Al_2O_3$ as catalyst on thermal decomposition of AN[15)]. Nano Al and $\gamma$-$Al_2O_3$ decreased the peak temperature of AN by 20°C and 7°C respectively. Vargeese investigated the catalysis of CuO, $TiO_2$, and LiF. The results indicated that $TiO_2$ almost showed no catalysis; CuO worked a little; LiF presented a negative effect on thermal decomposition of AN[16)]. Hasue studied the combustion performance of bis (1H-tetrazolyl) amine ammonium salt ($BTA \cdot NH_3$) and phase-stabilized ammonium nitrate (PSAN) mixture[17)]. He found that the mixture could be ignited at pressure of 1MPa, but the burning rate was very small (≤ 1 mm $s^{-1}$). The catalysis of NaCl, $BaCl_2$, and NaF on combustion of AN/GAP propellants were also probed by Sinditskii[18)]. He disclosed that the burning of propellants added with 7%NaCl could sustain at pressure of 0.5MPa, but the burning rate was still less than 1 mm $s^{-1}$. Miyata also confirmed that the mixture of AN and aminoguanidinium 5,5'-azobis-1H-tetrazolate (AGAT) (50/50) can be ignited at pressure of 0.5MPa, but the burning rate was only closed to 1 mm $s^{-1}$ [19)]. Although abovementioned results were unsatisfactory, the research about AN based propellants was rejuvenated.

Now we found that since 2011, the studies about AP decreased but the researches about AN increased. In particular the researchers from Russia, Japan, and India paid more attention on AN based propellants[20)–23)]. In this paper, after studied the decomposition mechanism of AP and AN in detail, we proposed that solid strong acid may exhibit good catalysis ability because their super high acidity may strongly promote the decomposition. So we enlisted TG-DTG-DSC and DSC-IR technology to affirm the suggestion.

## 2. Experimental

### 2.1 Sample preparation

With violent stirring, $Fe(NO_3)_3$ solution was dropped into 6 mol/L $NH_3 \cdot H_2O$ solution that originally contained 10% ethanol as dispersant agent. pH value was adjusted to 9-10, and then red brown precipitation ($Fe(OH)_3$) was obtained. After aging 24h, the precipitation was washed with $H_2O$ three times; then it was washed with ethanol two times; finally, it was washed with acetone one time. After lavation, the precipitation was dried at 50°C. The dried powder was carefully grinded in agate mortar, and then the amorphous $Fe_2O_3$ tiny particles were gained.

With stirring and ultrasonic, 2 g amorphous $Fe_2O_3$ was put into sulfuric acid solution and dipped in 30 min. After dipping, the amorphous $Fe_2O_3$ was filtrated out and dried at 80°C. The dried powders were grinded and calcined at 300°C, 400°C, 500°C, or 800°C, and then solid strong acids were obtained. This solid acid was marked as "$SO_4^{2-}$/$Fe_2O_3$".

In order to investigate the catalysis of $SO_4^{2-}/Fe_2O_3$ on decomposition of AP and AN, four samples were prepared. (1) 0.97 g AP was blended with 0.03 g $SO_4^{2-}/Fe_2O_3$ by carefully manual grinding, and the obtained sample was tagged as [AP+3%$SO_4^{2-}/Fe_2O_3$]. (2) For comparing, another 0.97 g AP was also blended with 0.03 g $Fe_2O_3$ by carefully manual grinding, and the gained sample was tagged as [AP+3%$Fe_2O_3$]. (3) 0.97 g AN was blended with 0.03 g $SO_4^{2-}/Fe_2O_3$ by carefully manual grinding, and the obtained sample was tagged as [AN+3%$SO_4^{2-}/Fe_2O_3$]. (4) For comparing, another 0.97 g AN was also blended with 0.03 g $Fe_2O_3$ by carefully manual grinding, and the gained sample was tagged as [AN+3%$Fe_2O_3$].

### 2.2 Methods and measurements

The morphology was observed with a field-emission scanning electron microscope (SEM, JEOL JSM-7500). The

phases of the samples were investigated with an X-ray diffractometer (XRD, Bruker Advance D8), using Cu K_$\alpha$ radiation at 40 kV and 30 mA. XPS analysis was performed by X-ray photoelectron spectroscopy (XPS), PHI5000 Versa-Probe (ULVAC-PHI). TG-DSC analysis and DSC-IR analysis were carried out by using a thermal analyzer system (TG/DSC, Mettler Toledo) coupled with a Fourier transform infrared spectrometer.

## 3. Results and discussion

### 3.1 Morphology and structure

The XRD analyses were performed and the results were illustrated in Figure 1. It was indicated that the amorphous powder did not transform into crystal phase after calcined at 300°C or 400°C. When the temperature climbed to 500°C, $\alpha$-$Fe_2O_3$ formed and its average grain size was 24.9 nm. When the temperature increased to 800°C, the peak intensity became very strong and its average grain size was more than 100 nm. In Figure 1 (b), XRD patterns of two samples were compared. One was the powder underwent surface acidification in sulfuric acid ($SO_4^{2-}/Fe_2O_3$), and another was the powder without surface acidification ($Fe_2O_3$). The result showed that the peak intensity of $Fe_2O_3$ was stronger than that of $SO_4^{2-}/Fe_2O_3$, which meant that surface acidification could retard the crystallization of $Fe_2O_3$. Average grain size of $Fe_2O_3$ was 29.8 nm.

Figure 2 (a) is the XPS spectrum of $SO_4^{2-}/Fe_2O_3$ that was the powder subjected to acidification in 0.3 mol/L sulfuric acid and calcined in 500°C (Figure 2 (b) is the expansion of Figure 2 (a)). In XPS spectrum, three elements of O, Fe, and S were detected. Fe and O peaks located at binding energy of 706.7eV and 529.9eV respectively, which should reflect to the elements in $Fe_2O_3$ because their peak intensity was very strong. The peak at binding energy of 168.5eV should relate to 2p electron transition of S element. The S element should origin from the $SO_4^{2-}$ radical on the surface of $SO_4^{2-}/Fe_2O_3$. This implied that $SO_4^{2-}$ had been fixed on the surface of $Fe_2O_3$ after acidification.

To disclose the micron morphology and particle size of $SO_4^{2-}/Fe_2O_3$, SEM analysis were performed and SEM images of samples with and without surface acidification were showed in Figure 3. Figure 3 (a) imaged the sample without acidification ($Fe_2O_3$). $Fe_2O_3$ with particles size of 30 ~ 40 nm were agglomerate. Figure 3 (b) indicated that particles size of $SO_4^{2-}/Fe_2O_3$ were at nano scale. $SO_4^{2-}/Fe_2O_3$ particles were also agglomerate each other. Therefore, we had enough reason to reconsider the drying process in fabrication of $SO_4^{2-}/Fe_2O_3$. Freeze-drying or supercritical drying may be more feasible. If we could use freeze-drying or supercritical technology to dry the power, we might obtain the particles with better dispersion. The particle size distribution was obtained by carefully measure the specific size of each particle in SEM images (Figure 3 (a) and Figure 3 (b)), in which the number of the particles that were gauged was more than 120 for each sample. The measurement was carried out by software based on Equation 1. Then the data were displayed as a statistic figure (Figure (3c) and Figure (3d)). It indicated that $Fe_2O_3$ and $SO_4^{2-}/Fe_2O_3$ have their mean particle size of 27 nm and 25 nm respectively. This was accordance with result in XRD analysis, i.e. surface acidification slightly retarded the growth of particles (or grains).

$$P(d) = \frac{A}{d\sigma_d\sqrt{2\pi}} \cdot \exp\left[-\frac{1}{2\sigma_d^2} \cdot \ln^2\left(\frac{d}{d_0}\right)\right] \quad (1)$$

where $P(d)$ is particle size distribution; $\sigma_d$ is the standard deviation of the diameters, $d_0$ is the mean diameter, $A$ is a constant.

### 3.2 Thermal analysis

Catalysis of $SO_4^{2-}/Fe_2O_3$ was probed with thermal analyses and the results were illustrated in Figure 4. Figure 4 (a) showed that DSC trace of raw AP comprised one endothermic peak and two exothermic peaks, which refer to the phase transformation and thermal decomposition of AP. For [AP+3%$Fe_2O_3$], the peaks for phase transformation and low temperature decomposition changed seldom compared with those of pure AP. The peak temperature of high temperature decomposition decreased by 35.1°C and the decomposition heats increased. For [AP+3%$SO_4^{2-}/Fe_2O_3$], compared with pure

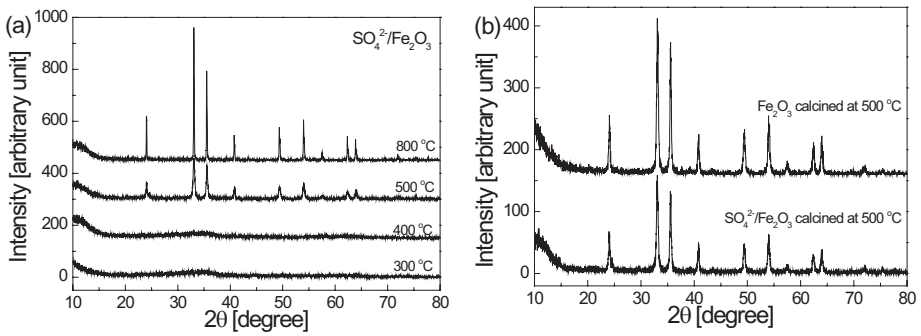


**Figure 1** XRD patterns of samples: (a) $SO_4^{2-}/Fe_2O_3$ calcined at different temperature; (b) $Fe_2O_3$ and $SO_4^{2-}/Fe_2O_3$ calcined at 500 °C.

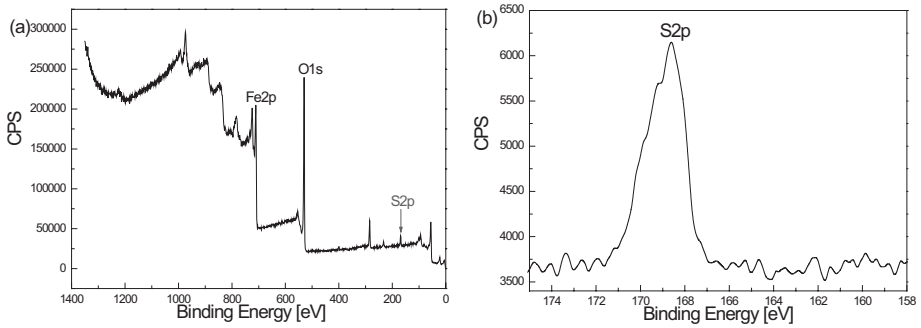


**Figure 2** XPS spectra of $SO_4^{2-}/Fe_2O_3$ nanoparticles. Figure 2 (b) is the expansion of Figure 2 (a).

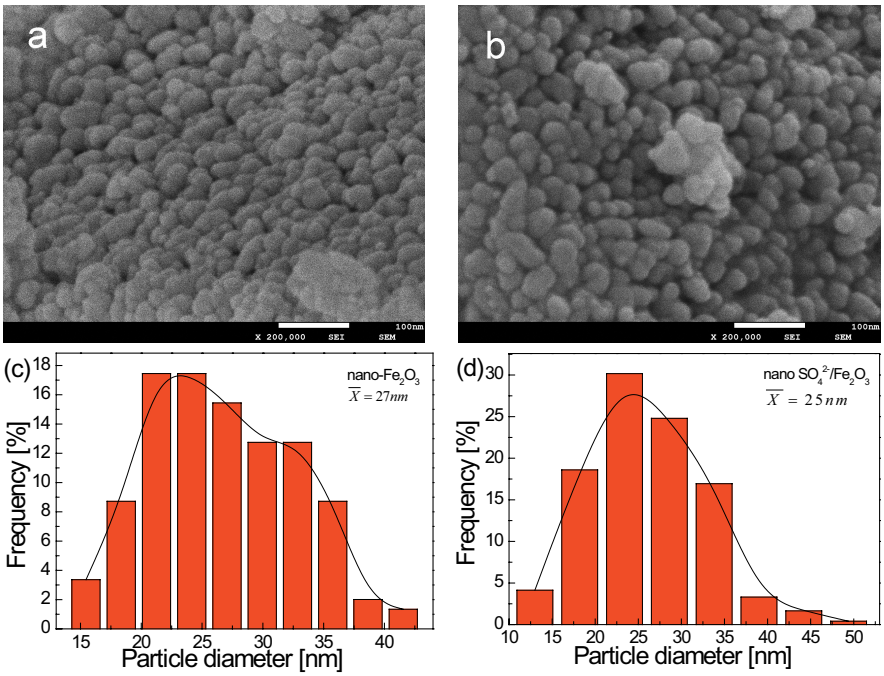


**Figure 3** SEM images of $Fe_2O_3$ (a) and $SO_4^{2-}/Fe_2O_3$ (b) nanoparticles calcined at 500 °C.

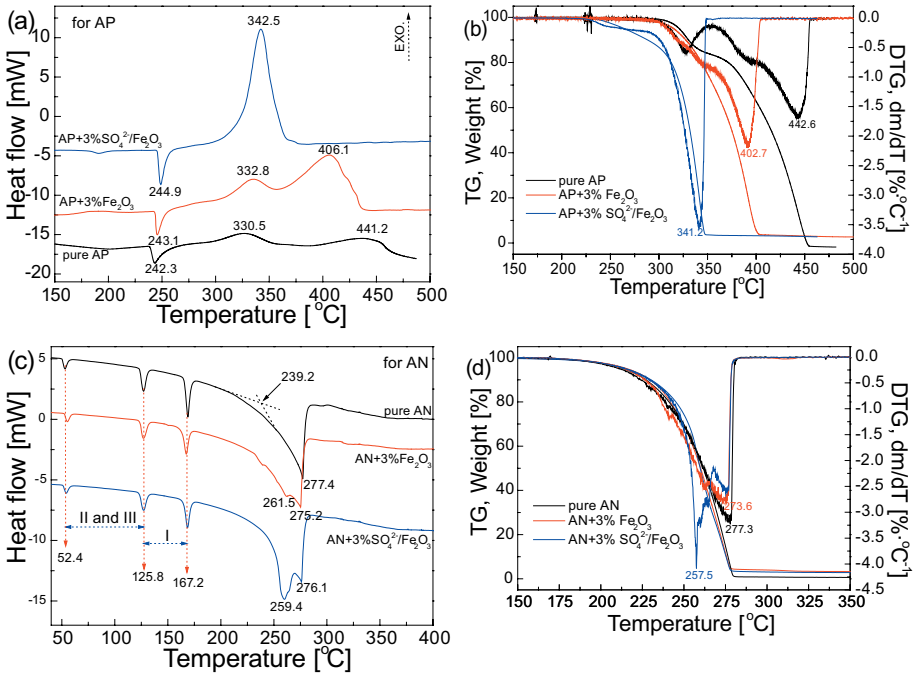


**Figure 4** DSC traces of samples: (a, b) for AP; (c, d) for AN.

AP, the phase transformation peak did not move but the exothermic peak temperature decreased by 98.7°C; meanwhile, the peaks for low and high temperature decomposition incorporated in one exothermic peak. These results meant that the catalysis action of nanometer $SO_4^{2-}/Fe_2O_3$ was higher than that of nano $Fe_2O_3$. Figure 4 (b) illustrated the TG-DTG curves of samples, in which the DTG curves were obtained by derivation calculus to TG curves. In terms of the curves, the difference among the samples was obvious. The DTG peak of [AP+3%$SO_4^{2-}$/$Fe_2O_3$] was stronger than others, and it was of the highest value of $|dm/dT|_{max}$. This implied that the decomposition rate of [AP+3%$SO_4^{2-}/Fe_2O_3$] was faster. The peak points in DTG curves, where the $|dm/dT|_{max}$ located, were closed to the peak points in DSC curves respectively.

Figure 4 (c) indicated that there were four endothermic peaks and no exothermic peaks in DSC trace of pure AN. The peak at 52.4°C reflected to a phase transformation (phase III to phase II, $\Delta H = 13.9$ J $g^{-1}$). The peak at 125.8°C also refer to a phase transformation (phase II to phase I, $\Delta H = 40.1$ J $g^{-1}$). The peak at 167.2°C related to melting course of AN ($\Delta H = 55.4$ J $g^{-1}$). The strongest endothermic peak reflected to thermal decomposition of AN. The decomposition began at 239.2°C and showed its peak point at 277.4°C ($\Delta H = 888.9$ J $g^{-1}$). As the first step of condense phase reaction, $NH_3$ (g) and $HNO_3$ (g) would form by dissociation of $NH_4NO_3$. This dissociation course would absorb heat of 2.18kJ·$g^{-1}$ [24]. Although subsequent reactions were exothermic, the released heat was less than 2.18kJ·$g^{-1}$. So, the whole decomposition of AN was endothermic. Therefore, pure AN can not be ignited in air or in $N_2$ because its decomposition is not self-sustained. This is why AN presents much low sensitivities. In addition, we could find that nanometer $Fe_2O_3$ and nanometer $SO_4^{2-}/Fe_2O_3$ did not change the decomposition process of AN, because the DSC curve of [AN+3%$Fe_2O_3$] or [AN+3%$SO_4^{2-}/Fe_2O_3$] also exhibited four endothermic peaks (two to phase transformation, one to melting, and one to thermal decomposition). This meant that adding nano catalyst could not change the reaction heats in thermodynamics. However, comparing with pure AN, the decomposition peak of AN doped 3%$SO_4^{2-}/Fe_2O_3$ decreased by 18.0°C; and the nano $Fe_2O_3$ almost showed no catalysis because the peak temperature only decreased by 2.2°C. This meant that the existence of $SO_4^{2-}$ (instead of pure $Fe_2O_3$) favored to thermal decomposition of AN. Figure 4 (d) showed the TG-DTG curves of pure AN, [AN+3%$Fe_2O_3$], and [AN+3%$SO_4^{2-}/Fe_2O_3$]. There was not distinct difference in TG curves. After derivation calculus, the DTG curves were gained and the curve depicted the decomposition rate of samples. Their DTG peak profile was as similar as that of DSC peaks.

### 3.3 Catalysis mechanism

By means of DSC-IR analysis, we investigated decomposition products for [AP+3%$SO_4^{2-}/Fe_2O_3$] and [AN +3%$SO_4^{2-}/Fe_2O_3$] and the results were showed in Figure 5. For [AP+3%$SO_4^{2-}/Fe_2O_3$], we intercepted the IR spectra at 221.8°C, 296.1°C, 341.5°C, 346.8°C, and 351.9°C, respectively. From Figure 5 (b), it was found that the decomposition products were $NO_2$, NOCl, $N_2O$, $HClO_4$, NO, HCl, and $H_2O$. In particular, the peak intensity of $NO_2$, NOCl, and $N_2O$ were much stronger than that of others. In Reference[25], $Cl_2$ and $O_2$ usually formed in decomposition of AP. However, these non-polar molecules can not be detected by IR technology. Thus, we also considered there were some $Cl_2$ and $O_2$ generated. According to the products, the decomposition reactions of [AP+3%$SO_4^{2-}/Fe_2O_3$] were deduced (i.e. Equations 2 and 3). Obviously, despite existence of some $HClO_4$, $NH_3$ were not detected in the products. It meant that the oxidation of $NH_3$ proceeded very completely. We inferred that the generated $NH_3$ gas adsorbed on the surface of AP and nanometer $SO_4^{2-}/Fe_2O_3$. Especially, when $pK_a(SO_4^{2-}/Fe_2O_3)$ was much lower than $pK_a(NH_3)$, the reaction of $NH_3+H^+ \rightleftharpoons NH_4^+$ occurred (The parameter "$pK_a$", which can be used to quantify the strength of an acid, is called acidity coefficient. Each acid has its own "$pK_a$" value.). This reaction meant that a part of $NH_3$ could be fixed as condense phase on the surface of nanometer $SO_4^{2-}/Fe_2O_3$. This benefited to the oxidation of $NH_3$ because it avoided the cessation of AP decomposition by $NH_3$ poisoning. Hence, the decomposition of [AP+3% $SO_4^{2-}/Fe_2O_3$] only showed one exothermic peak in DSC trace.

$$NH_4ClO_4 \rightleftharpoons NH_3(s)+HClO_4(s) \rightleftharpoons NH_3(g)+HClO_4(g) \quad (2)$$

$$5NH_3+5HClO_4 \rightarrow NO_2+N_2O+NO+2HCl+NOCl+Cl_2+3O_2+9H_2O \quad (3)$$

For [AN+3%$SO_4^{2-}/Fe_2O_3$], we intercepted the IR spectra at 161.5°C, 215.7°C, 238.8°C, 264.9°C, 286.3°C, and 345.7°C, respectively (in Figure 5 (b)). Figure 5 (d) revealed that the decomposition products of [AN+3%$SO_4^{2-}/Fe_2O_3$] were $N_2O$ and seldom $H_2O$. This meant the decomposition proceeded very completely. In theory, decomposition of AN complies with ionic reactions (Equations 4~7) or radical reactions (Equations 8~10). The gas product of both the channels was $N_2O$, which consisted with our experimental results. Distinctly, at low temperature, thermal decomposition of AN would comply with ionic reactions since the rupture of O-N bond (i.e. Equation 8 would happen only at temperature more than 1300°C. In ionic mechanism, the reaction of Equation 5 was the limiting step because their rate constants were very small. So if we introduced some strong acid (HA, $pK_a$ (HA) < $pK_a(HNO_3)$) into the decomposing AN, the reaction of $NO_3^- + H^+ \rightleftharpoons HNO_3$ would happen due to the principle of chemical replacement of weak acid by strong acid. This would considerably increase the concentration of $HNO_3$ in the decomposition system, which resulted in a remarkable promotion on the key reactions (i.e. Equations 5~7). Therefore, the decomposition of AN was accelerated. Especially, when $pK_a$ (HA) $\ll pK_a$ ($HNO_3$), the decomposition of $HNO_3$ would be changed (see Equation 11).

$$NH_4NO_3 \rightarrow NH_3+HNO_3+2.18kJ/g \quad (4)$$

$$2HNO_3 \rightleftharpoons [NO_2^+ NO_3^-]+H_2O \quad (5)$$

$$[NO_2+NO3^-]\ NO_2^+ + NO_3^- \quad (6)$$

$$NO_2^+ + NH_3 \rightleftharpoons [NH_3 \cdot NO_2^+] \rightarrow N_2O+H_3O^+ \quad (7)$$

$$HNO_3 \rightarrow \cdot OH+NO_2 \quad (8)$$

$$NH_3+\cdot OH \rightarrow \cdot NH_2+H_2O \quad (9)$$

$$NH_2+NO_2 \rightarrow [NH_2NO_2] \rightarrow N_2O+H_2O \quad (10)$$

$$HNO_3+H^+ \rightleftharpoons [H_2ONO_2]^+ \rightarrow NO_2^+ + H_2O \quad (11)$$

The "strong acids" are several kinds of solid acids whose acidity are much higher than that of 100% $H_2SO_4$. Generally, their $pK_a$ are less than -11.93[26),27]. In industry, many organic synthesis reactions must use acid as catalyst. Comparing with liquid acid, solid acids are of advantages such as high catalysis, high selectivity, pollution-free, as well as easy to separate from reaction system. Thus, they have a bright application prospect in organic industry. Mainly, there are four kinds of solid acid that are classified as strong acid. Kind 1 is the supported heteropoly acids, such as HF-$SbF_5$-$AlF_3/Al_2O_3$, $SbP_3$-Pt/Graphite, $SbP_3$-HF/F-$A1_2O_3$, $SbF_5$-$FSO_3H$/Graphite, and so on. Kind 2 is the mixture of inorganic salts, such as $AlCl_3$-$CuCl_2$, $MCl_3$-$Ti_2(SO_4)_3$, $A1C1_3$-$Fe_2(SO_4)_3$, and so on. Kind 3 is

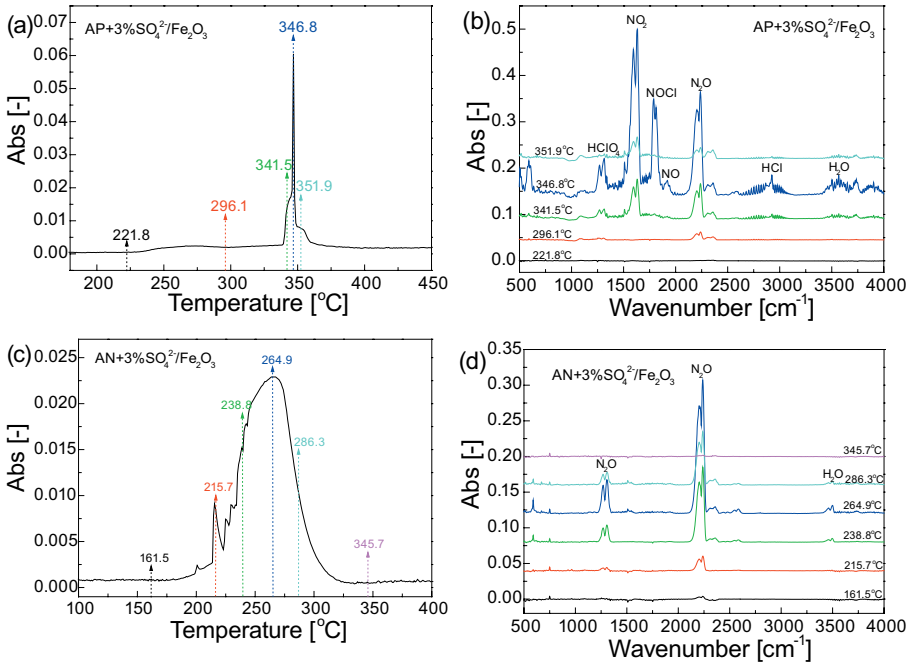


**Figure 5** IR spectra of decomposition products: (a, b) [AP+3%$SO_4^{2-}/Fe_2O_3$]; (c,d) [AN+ 3%$SO_4^{2-}/Fe_2O_3$]; (a, c) are total absorbance of gas products; (b, d) are IR spectra of gas products intercepted at different temperature (the temperature nodes of interception were illustrated in Figure 5 (a) and (c), respectively.).

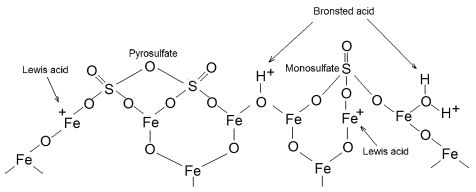


**Figure 6** Proposed surface structural model and strong-acid species on the surface of $SO_4^{2-}/Fe_2O_3$ acid.

acid metal oxide coated with $SO_4^{2-}$, such as $SO_4^{2-}/ZrO_2$, $SO_4^{2-}/TiO_2$, $SO_4^{2-}/Fe_2O_3$, etc. Kind 4 is composition of metal oxides, such as $WO_3/ZrO_2$, $MoO_3/ZrO_2$, etc. All the solid strong acids show their $pK_a$ are less than -10 at lest. However, the reason why they process of so strong acidity is obscure. Meanwhile, the different kind of strong acid may have different reason. In my study, we pay more attention to the strong acid of kind 3, because it can be easily prepared and their particle sizes are easily controlled in nanometer scale. According to the studies of Guo[28] and Wang[29], they considered that due to the strong inductive effects of S=O group, the adsorbed $H_2O$ contributes as Brϕnsted acid center. The surface acid sites are associated with the metal ions whose acidic strength can be strongly enhanced by induction effect of S=O groups (please see Figure 6).

In addition, solid strong acids do not like traditional acids that can form a mass of $H^+$ ions when they dissolve into water. For solid strong acid, Brϕnsted acid centers are only existent on their surface. The centers work only if the molecular of reactant(s) absorbed on the surface of the catalyst. Thus, this kind of catalysis is not homogeneous catalysis but rather heterogeneous catalysis. Of course, the acid groups on the surface of solid strong acid can be "apperceived" by the reactions with some chemical agents. For example, a suitable method for determining the acid strength of solid acid may be "Steam Method" reported by Li[26]. In Li's study, the agents, such as m-nitrotoluene ($pK_a = -11.99$), p-nitrochlorobenzene ($pK_a = -12.70$), m-nitrochlorobenzene ($pK_a = -13.60$), and dinitrofluorobenzene ($pK_a = -14.52$), were used as indicators.

In fact, for solid strong acid, its preparation method and the acid strength (very high) had become a common recognition early. Thus, this paper took more efforts on the catalysis ability and catalysis mechanism of solid strong acid on thermal decomposition of AP and AN. As for the property and the function of these acid groups (on the surface of solid acid particles), I think these had been clearly elucidated in many references (just like Reference[26)–29)]).

In fact, plenty of Lewis acid points and Bronsted acid points were co-existent on the surface of nanometer $SO_4^{2-}/Fe_2O_3$. However, what really matters was not Lewis acid but Bronsted acid because pure nano $Fe_2O_3$ did not present some catalysis action (there are so many Lewis acid points on the surface of nano $Fe_2O_3$). The liquid $H_2O$, which generated from decomposition of AN, could enable the transformation (Lewis acid transforms to Bronsted acid). However, the liquid $H_2O$ could also make the $SO_4^{2-}$ lose from the surface. Thus, the $H_2O$ in condense phase could obviously weaken the catalysis of nanometer $SO_4^{2-}/Fe_2O_3$. In fact, Sun et al had reported that some inorganic acids such as concentrated sulfuric acid and concentrated hydrochloric acid could promote the decomposition of AN; and the catalysis action of hydrochloric acid were distinctly higher than that of sulfuric acid[26]. The catalysis mechanism of inorganic acids had been elucidated above. But we can not added liquid acid into a propellant because the processing property of the propellant will be deteriorated. Hence, using solid acid may be a better choice. Moreover, in terms of acidity, the $p\,K_a$ of solid strong acid (~−14) was far less than $p\,K_a$ of sulfuric acid ($p\,K_a = -3.0$) and hydrochloric acid ($p\,K_a = -8.0$). Thus, solid strong acid may show higher catalysis action than those liquid acids. Meanwhile, the processing property of propellants will not be affected by adding little solid strong acid.

Overall, the catalysis action of $SO_4^{2-}/Fe_2O_3$ nanoparticles was not as excellent as expectation. According to the reported studies, its catalysis ability should be lower than metal nanoparticles (especial nano Cu) but higher than traditional metal oxides. However, owing to the very low cost in fabrication and storage, using solid strong acids as catalysts is worthy to be attempted. Moreover, there are so many kinds of solid strong acid that could exhibit different catalysis ability. Hence, this study is just a beginning of these.

## 4. Conclusions

$SO_4^{2-}/Fe_2O_3$ nanoparticles were prepared by precipitation-dipping method. XRD analysis indicated that the amorphous $Fe_2O_3$ transformed to $\alpha$-$Fe_2O_3$ after calcined at 500°C. By using JADE5.0 software, the average grain size of $SO_4^{2-}/Fe_2O_3$ was calculated. SEM images showed that the particle size of $SO_4^{2-}/Fe_2O_3$ was 30-40 nm. XPS analysis presented that after acidification, the $SO_4^{2-}$ was fixed well on the surface of $Fe_2O_3$.

Thermal analyses were performed to probe thermal decomposition of [AP+3%$Fe_2O_3$], [AP+3%$SO_4^{2-}/Fe_2O_3$], [AN+3%$Fe_2O_3$], and [AN+3%$SO_4^{2-}/Fe_2O_3$]. The results indicated that $SO_4^{2-}/Fe_2O_3$ presented higher catalysis than nano $Fe_2O_3$. DSC-IR analyses were employed to detect the gas products for thermal decomposition of [AP+3%$SO_4^{2-}/Fe_2O_3$] and [AN+3%$SO_4^{2-}/Fe_2O_3$]. Via analyzing the IR spectra of gas products, we found that the gases such as $NO_2$, NOCl, $N_2O$, $HClO_4$, NO, HCl, and $H_2O$ generated in decomposition of [AP+3%$SO_4^{2-}/Fe_2O_3$]. For [AN+3%$SO_4^{2-}/Fe_2O_3$], the main gas products were $N_2O$ and seldom $H_2O$, which meant that the decomposition reaction proceeded very completely. According to the detected products, the possible decomposition mechanism of AP and AN were derived. Meanwhile, the catalysis actions of $SO_4^{2-}/Fe_2O_3$ were discussed in detail.

## Acknowledgement

This research was supported by the National Natural Science Foundation of China (Grant No.: 51206081; Recipient: Yi Wang). Second author (Yi Wang) paid the

same effort and contribution to this paper as the first author (Xiaolan Song).

## References


1) Oide Sho, Takahashi Kenichi, and Kuwahara Takuo, Sci. Tech. Energetic Materials, 73, 153−156 (2012).
2) Kohga Makoto, Sci. Tech. Energetic Materials, 71, 145−150 (2010).
3) A. P. Sanoop, R. Rajeev, and B. K. George, Thermochim. Acta, 606, 34−40 (2015).
4) Y. H. Wang, T. Xu, and L. L. Liu, Sci. Tech. Energetic Materials, 75, 21−27 (2014).
5) Kakami Akira, Terashita Shota, and Tachibana Takeshi, Sci. Tech. Energetic Materials, 70, 145−151 (2009).
6) S. Singh, G. Singh, and N. Kulkarni, J. Therm. Anal. Calorim., 119, 309−317 (2015).
7) Fujimura Kaori and Miyake, Sci. Tech. Energetic Materials, 69, 149−154 (2008).
8) K. Gao, G.P. Li, and Y.J. Luo, J. Therm. Anal. Calorim., 118, 43−49 (2014).
9) Fujimura Kaori and Miyake Atsumi, Sci. Tech. Energetic Materials, 71, 65−69 (2010).
10) G. Z. Hao and J. Liu, Propellants Explos. Pyrotech., 40, 848−853 (2015).
11) Ohtake Toshiakim, Date Shingo, and Ikeda Ken, Sci. Tech. Energetic Materials, 76, 1−2 (2015).
12) Hasue Kazuo, Sci. Tech. Energetic Materials, 75, 5−6 (2014).
13) C. Oommen and S. R. Jain, J. Hazard. Mater., A67, 253−281 (1999).
14) T. Naya and M. Kohga, Propellants Explos. Pyrotech., 38, 87−94 (2013).
15) V. N. Popok and N. V. Bychin, Nanotechnol. Russ., 9, 541−548 (2014).
16) A. A. Vargeese, S. J. Mija, and K. Muralidharan, J. Energ. Mater., 32, 146−161 (2014).
17) K. Hasue, J. Energ. Mater., 32, 199−206 (2014).
18) V. P. Sinditskii and V. Y. Egorshev, Propellants Explos. Pyrotech., 30, 269−280 (2005).
19) Y. Miyata and K. Hasue, J. Energ. Mater., 29, 344−359 (2011).
20) V. P. Sinditskii and V. Y. Egorshev, Combust. Explo. Shock Waves, 48, 81−99 (2012).
21) T. Naya and M. Kohga, J. Energ. Mater., 33, 73−90 (2015).
22) M. Kohga and K. Okamoto, Combust. Flame, 158, 573−582 (2011).
23) S. Chaturvedi and P. N. Dave, J. Energ. Mater., 31, 1−26 (2013).
24) R. Gunawan and D. K. Zhang, J. Hazard. Mater., 165, 751−758 (2009).
25) P. W. M. Jacobs and G. S. Pearson, Combust. Flame., 13, 419−430 (1969).
26) Q. Y. Li, Petrochemical Technol., 34, 75−77 (2005).
27) R. R. Zhan, Chin. Rare Earths, 3, 84−88 (2009).
28) H. F. Guo, Mater. Chemist. Phys., 112, 1065−1068 (2008).
29) Y. Wang, J. Mater. Sci., 44, 6736−6740 (2009).
30) J. H. Sun, Z. H. Sun, and Q. S. Wang, J. Hazard. Mater., 127, 204−210 (2005).